LETTER

Buried Interface Passivation of Perovskite Solar Cells by Atomic Layer Deposition of Al$_2$O$_3$

Sudeshna Ghosh, Debasmita Pariari, Tejmani Behera, Pablo P. Boix, Narasimha Ganesh, Susmita Basak, Arya Vidhan, Nisha Sarda, Iván Mora-Seró, Arindam Chowdhury, Kavassery Sureswaran Narayan, D. D. Sarma,* and Shaibal K. Sarkar*

Cite This: *ACS Energy Lett.* 2023, 8, 2058−2065

Read Online

ACCESS | Metrics & More | Article Recommendations | SI Supporting Information

ABSTRACT: Despite having long excited carrier lifetimes and high mobilities in hybrid halide perovskite materials, conventional (n-i-p) devices exhibit significant interfacial nonradiative recombination losses that are little understood but limit the radiative efficiency and the overall open-circuit potential. In this Letter, we reveal that the process of spiro-OMeTAD coating on perovskite gives rise to buried defect states, which are detrimental to the devices' operational stability. We subsequently report a method to passivate these deleterious buried defect states by atomic layer deposition of Al$_2$O$_3$ through controlled precursor dosages on fully functional devices. The process results in notable improvements in the overall device performance, but the underlying root-cause analysis is what we essentially aimed to elucidate here. The reported passivation technique results in (a) an increase in the efficiency primarily due to an increase of V_{OC} by ∼60−70 mV and consequently (b) enhanced photoluminescence and higher electroluminescence quantum efficiency and (c) overall device operational (MPPT) stability under ambient and, exclusively, even under high vacuum (>300 h) conditions, which is otherwise challenging.
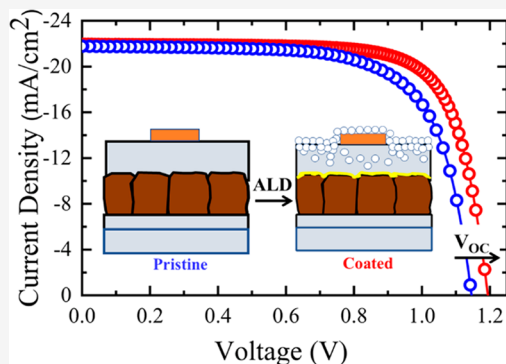
During the past decade, the meteoric rise in hybrid halide perovskite devices is largely credited to a well-orchestrated rational development of the material and device processing methods.[1,2] With substantial development in the solution chemistry, bulk defects in the perovskite materials are effectively reduced as the estimated quasi-Fermi level splitting (QFLS) in the bulk is near to the thermodynamic limit, but the obtained open-circuit potential is significantly lower than its radiative limit.[3] This is due to either the polycrystallinity nature of the absorber layer which induces large defect density at the grain boundaries or, importantly, the process-induced interfacial defects that are yet largely uncovered.[4] Evidently enough, the introduction of the charge transport layer(s) reduces the spread of the QFLS across the absorber layer, which is apparently due to the introduction of nonradiative recombination pathways at the interface, which in turn compromise the operational stability of the devices.[5] Thus, for the optimal development of the device, both in terms of efficiency and operational stability, identifying the root cause of the interfacial defects and thereafter minimization of the nonradiative recombination centers at the interface is an essential step to be fulfilled.

As a major avenue to passivate the interfacial defects, many pathways are explored.[6−8] Self-assembled monolayers at the base oxide materials (SnO$_2$[9] or TiO$_2$[10] for the n-i-p structures or NiO$_x$[11] for the p-i-n structure) and perovskite interface have proven to be one of the effective ways to minimize the interface defects. The use of a bifunctional molecular layer at the oxide−perovskite interface passivates the interfacial defects, and the halide (or quasi-halide) termination helps the perovskite nucleation process.[12] In addition, the defect passivation at the halide perovskite and hole transport layer (HTL) interface is specifically targeted by the 2D (or even quasi-2D) perovskite layers. The presence of the interfacial 2D-perovskite layer not only enhances the optoelectronic properties of the device but also augments the operational stability.
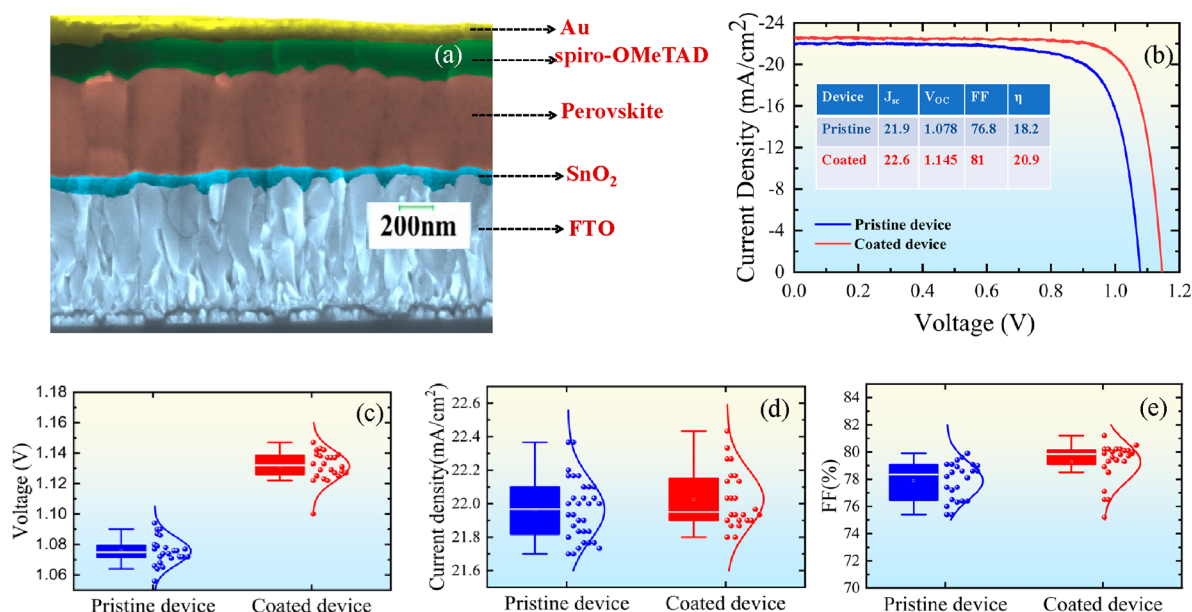
Figure 1. (a) Cross-sectional SEM image of the device architecture FTO/Bilayer SnO$_2$/Triple cation mixed halide perovskite/Spiro-OMeTAD/Au. (b) Light $J-V$ characteristics of pristine and ALD Al$_2$O$_3$ coated perovskite devices. (c) Statistical distribution of V_{OC} for pristine and coated devices. (d) Statistical distribution of current density for pristine and coated devices. (e) Statistical distribution of fill factor for pristine and coated devices. Please note that the device area is ~0.12 cm^2, but for the measurements, we used a shadow mask of an area of 0.03 cm^2.

From the early days of halide perovskite photovoltaics, atomic layer deposition (ALD) has been used as a tool to deposit/modify at either the ETL–perovskite[13] or HTL–perovskite[14] interface, aiming to reduce the interfacial recombination losses, but pieces of evidence regarding either chemical or field-effect passivation are still largely lacking in the literature. Due to the chemical incompatibility, ALD on perovskite is found to be more challenging.[15,16] We have previously shown that there is a preferential etching of the organic moiety by the metalorganic precursors during the ALD process, leaving behind the PbI$_2$,[15] which was also subsequently reported by several other groups.[16,17] However, whether the PbI$_2$ formation at the grain boundaries is found to be beneficial or not is still questionable,[18] though preferred,[19] but the uncontrolled formation of the same is unquestionably disadvantageous for the device performance.

Here, we report that the Li-TFSI-doped spiro-OMeTAD (hole-transporting layer, HTL) coating on multication-halide perovskite induces metastable defects at the interfaces, which is detrimental to the photovoltaic devices' operational and shelf stability. Furthermore, to negate the defects, we introduce a process after device assembly to reduce the nonradiative recombination at the buried interface. A substrate-enhanced ALD of Al$_2$O$_3$ is employed on a fully functional device that helps to passivate the HTL–perovskite interface with controlled PbI$_2$ formation. The process essentially improves the open-circuit potential (V_{OC}) by ~70 mV, resulting in a ~12% increment in the overall device efficiency and, consequently, an order of magnitude improvement in the electroluminescence (EL) quantum yield. The passivated devices offer higher operational stability not only in ambient but also under high-vacuum conditions, which is an exclusive advantage against the commonly employed passivation processes with a lower-dimensional perovskite layer.

This investigation is based on standard perovskite devices with n-i-p architecture with multication multianion hybrid perovskite (($(FA_{0.83}MA_{0.17})_{0.95}Cs_{0.05}PbI_{2.5}Br_{0.5}$) as the absorber material, designated as i-layer, which is sandwiched between the carrier selective layers as shown in Figure 1a (cross-sectional SEM image). For the electron transport layer (ETL), bilayer SnO$_2$ (blocking and colloidal layer) is used while Li-TFSI doped spiro-OMeTAD (spiro) is employed as the HTL (see the Supporting Information, Experimental Section). The photoconversion efficiencies of as-prepared devices lie in the range of 18−20%, and considering the aim of this report, we have not put much emphasis on device optimization. The Al$_2$O$_3$ ALD coating on the as-prepared devices is conducted in a custom-built setup,[20] at 70 °C with alternate dosing of trimethyl aluminum (TMA) and H$_2$O. For the discussion below, it is worth mentioning here that these devices (both pristine and coated) do not show any measurable hysteresis (see Figure S1); thus, for ease in illustration we show only the reverse $J-V$ scans to represent the photovoltaic characteristics.

Figure 1b shows the light current−voltage ($J-V$) characteristics of a representative device before (pristine) and after the ALD (coated device). As depicted, the ALD coating yields an increase of 67 mV in the V_{OC} resulting in an increment of the device efficiency from 18.2% to 20.9% for the optimal-performing devices. Notably, the increase in the short-circuit current density (J_{SC}) is relatively slender, from 21.9 to 22.6 mA.cm^{-2}, and so is that of the fill factor (FF), from ~77% to 81%. Thus, the increase in the V_{OC} upon ALD coating is the major responsible factor for the device efficiency enhancement (see Figures S2 and S3). Figure 1c−e shows the photovoltaic parameters inferred from the $J-V$ measurements from 30 different samples before and after the ALD coating which statistically verify the trends mentioned above.

To understand the enhancement of V_{OC} between the pristine and the Al$_2$O$_3$-coated devices, we performed steady-state photoluminescence (PL) studies, both microscopy (see Schematic S1) and spectroscopy under open-circuit conditions. The room-temperature PL images shown in Figure S5
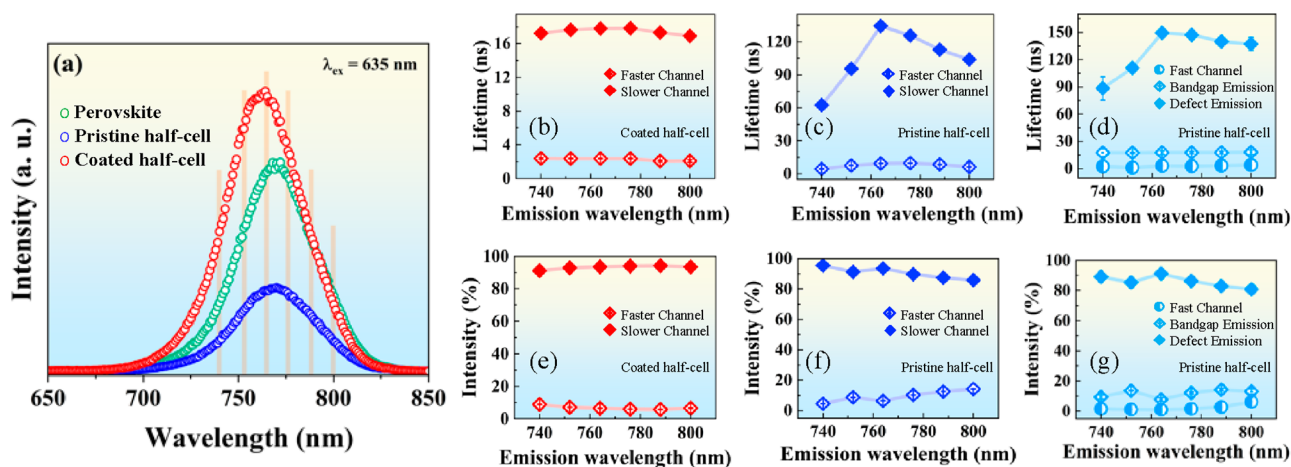
Figure 2. (a) Room-temperature PL spectra collected on the perovskite film (green circles), pristine (blue circles), and ALD coated (red circles) half-cells with the excitation wavelength as indicated. The yellow vertical lines mark the emission wavelengths where lifetime measurements were carried out. Extracted lifetimes as functions of the emission wavelength (b) from biexponential fittings for the coated half-cell, (c) from biexponential fittings for the pristine half-cell, and (d) from triexponential fittings for the pristine half-cell. Relative contributions of different decay channels as percentages of the total PL intensity for (e) the coated half-cell, (f) the pristine half-cell both with biexponential fittings, and (g) the pristine half-cell with triexponential fittings. Typical error bars on the estimates of the quantities shown in panels b−g arising from the fitting of the lifetime measurements are typically smaller than the symbol sizes.

make it visibly obvious that the ALD coating enhances the PL intensity of the device. Considering the measurement conditions (at steady state and under open circuit) and the fact that perovskite devices are primarily nonexcitonic devices, the observed increase in the PL intensity upon ALD coating corresponds to the larger quasi-Fermi level splitting (QFLS) and that in turn results in the higher V_{OC} that we observed. Considering that there is little increase in the J_{SC} after the ALD coating, it is highly unlikely that the ALD Al_2O_3 coating on top of the device can influence the defect concentration in the bulk of the absorber material, which is otherwise uniformly distributed throughout the thickness of the material. Such observations naturally lead to the assumption that the spatial location of the nonradiative recombination centers arising from interfacial defects is more likely to be affected by the ALD process.

To probe the presence of defect states influencing the overall photoexcited charge carrier dynamics, we did time-resolved PL (TRPL) studies on the pristine and coated devices. Notably, for the ease of interpretation and considering the obvious assumption, explained previously, that the said ALD process is unlikely to have any effect on the ETL or at the ETL− perovskite interface (see Figure S4), we hence used the half-cell configuration (glass/perovskite/spiro) for these measurements. Considering the room-temperature emission spectra with a significant phononic broadening (see Figure 2a), a clear separation between the signatures of the defect states and the bandgap emissions is difficult. Hence, we have carried out the TRPL studies at several photon energies[21] that are marked in Figure 2a with yellow vertical lines. Here, the change in the decay lifetime across the spectral width can give us important insight into the origins of de-excitation and therefore, on the presence of defect states. The PL intensity profile as a function of the decay time at each wavelength and its analysis are presented in the Supporting Information (Figures S6−S8, Tables S1−S3, and associated discussion).

We found that all time-dependent PL intensity data for the coated sample can be reliably fitted with two time scales, with a short lifetime in the order of 2.25 ± 0.004 ns contributing less

than 10% of the total decay and a dominant one (>90% of the decay) with a lifetime of 17.74 ± 0.211 ns (see Figure S6 and Table S1). Plots of the two lifetimes and their relative contributions as percentages of the total PL intensity are shown as a function of the PL wavelength in Figure 2b,e.

The PL intensity decay for the pristine device could also be fitted with two lifetimes at each of the chosen wavelengths (see Figure S7 and Table S2), and the resulting lifetimes and relative contributions for the pristine device are shown in Figure 2c,f. Ignoring the minor contributions from the similarly short (~2 ns) lifetime processes for both samples, the remarkable difference in the lifetime of the majority process is that it is essentially constant (~17.00 ± 0.21 ns) and independent of the wavelength for the coated sample, while it shows a systematic increase from a relatively low value of 35 ns at the shortest wavelength, reaches the highest value of 134 ns, and then decreases more modestly to 104 ns as a function of the wavelength. Such large values of the lifetime point to defect states being primarily responsible for these majority decay channels in the pristine sample. However, to elucidate the expected overlapping contributions from the bandgap emissions, we carried out a three-lifetime fitting of the PL decay plots of the pristine samples (see Figure S8 and Table S3 for details), and the corresponding data are shown in Figure 2d,g. This analysis clearly reveals that there is indeed a bandgap emission with a shorter lifetime of ~17.00 ± 0.21 ns that is essentially independent of the wavelength. This lifetime compares very well with the majority decay channel obtained for the coated sample, though the relative contribution of this bandgap emission channel drops from above 90% in the coated sample to ~11.68 ± 2.35% for the pristine sample. The majority of the decay in the pristine channel follows the longer decay time associated with overlapping defect states. These results suggest that the ALD coating leads to significant suppression of the defect states introduced at the level of preparing the pristine device, as also discussed below.

Furthermore, to identify spectrally resolved contributions from these two channels (band-edge and defect emission), lower-temperature (100 K) PL emission was performed where
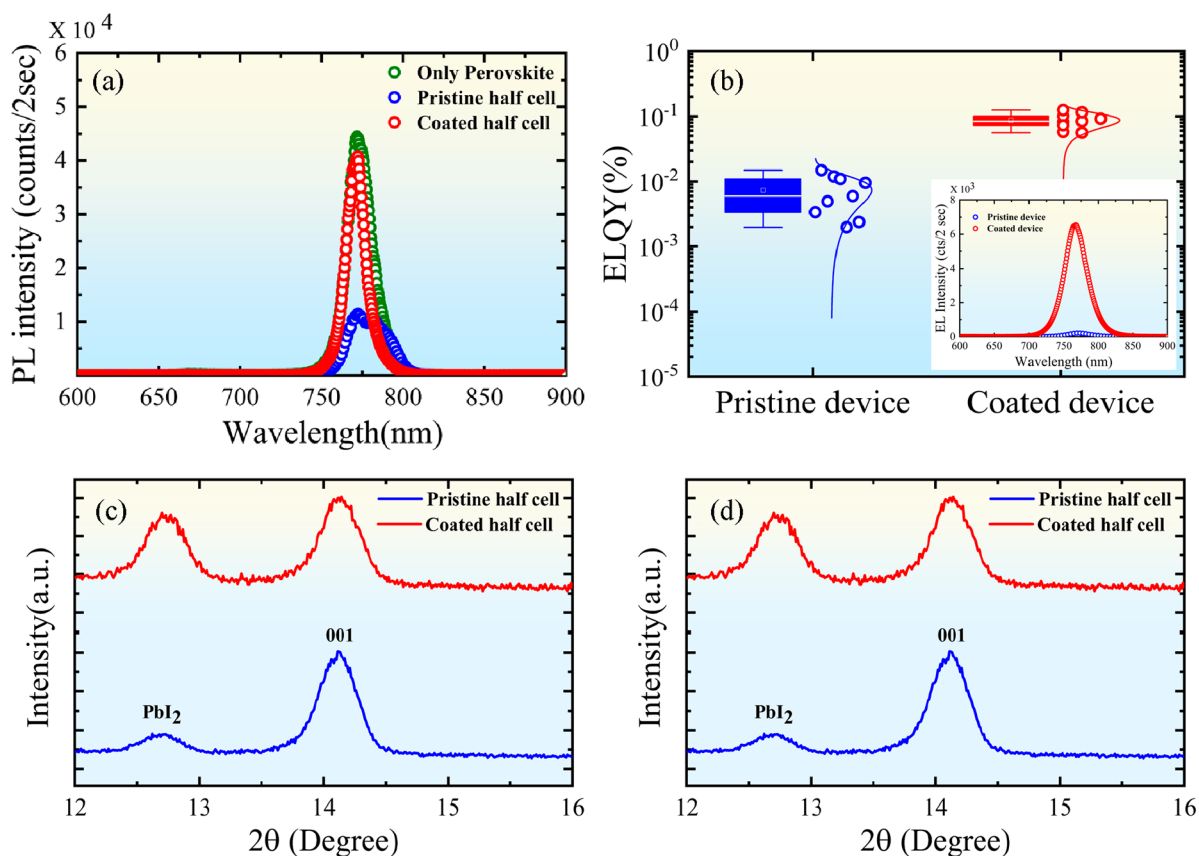
Figure 3. (a) PL spectra collected on the perovskite films (green) and pristine (blue) and ALD coated (red) half-cells at 100 K. (b) EL quantum yield (ELQY) collected on pristine (blue) and coated (red) devices. [The inset shows room-temperature EL spectra collected on pristine (blue) and coated (red) devices.] (c) XRD studies under grazing angle (0.5° incidence) obtained from pristine (blue) and coated (red) half-cells. (d) Bragg−Brentano (θ−2θ) mode XRD obtained from pristine (blue) and coated (red) half-cells.

defect emission distinguishable from the bandgap emission[22] is observed as shown in Figure 3a. The figure clearly shows a shoulder in the PL spectra at ∼785 nm (see Figure S9a−c for spectral deconvolution) only for the pristine device sample and is absent for both the pristine perovskite and the coated device; in other words, this longer wavelength feature appears only after the spiro coating, suggesting that this step in the device construction introduces extensive defect states at the interface affecting the optoelectronic properties adversely.

In addition, it is also indicated in Figure 3a that the PL intensity of the pristine perovskite is significantly reduced on making the pristine device with the spiro overlayer. Interestingly, upon ALD coating the PL signal associated with the defect states at ∼785 nm is completely removed and there is a significant enhancement of the primary PL peak centered at ∼770 nm. Intriguingly, for the coated half-cell, the full width at half maxima (fwhm ≈ 15 nm) of the emission peak is even lower than that of the pristine perovskite films (∼19 nm). Notably, in the coated half-cell devices the high-energy side of the spectra coincides with the pristine perovskite material, but the low-energy end is slightly blue-shifted, indicating the reduction of the intrinsic grain boundary defects in the perovskite materials, while the coated device appears to show dominantly the bandgap emission even at this lower temperature, consistent with our findings at room temperature.

To gain an understanding of the correlation between the V_{OC} improvement and the radiative versus nonradiative recombination, we opted for electroluminescence (EL)

measurements at a constant current equal to the J_{SC} of similar devices before and after the ALD. We find an order of magnitude increase in the EL quantum yield (ELQY) as shown in Figure 3b (measured ELQY as a function of the applied current is shown in the Supporting Information; see Figure S10 and the discussion there), and the corresponding representative spectra are shown in the inset. Since the EL signal majorly depends on the effective charge carrier injection (and hence the interfacial defects), the enhancement in the EL signal essentially accords with our conclusion from the PL analysis, explained above. Furthermore, from the reciprocity theorem (see the Supporting Information for details), we estimated the voltage losses between the pristine and coated sample as 62 ± 7 mV (see Table S4), which is similar to the one measured from J−V measurements (see Figure 1).

The PL and EL-based measurements and analysis indicate the presence of an improved perovskite−HTL interface which is the key factor responsible for reduced nonradiative V_{OC} loss. We investigated the physical origin of this passivation of the buried perovskite−HTL interface from a fundamental standpoint to decipher the role of ALD of Al_2O_3 in this process. Undoubtedly, the primary motivation for having Al_2O_3 by ALD on the fully functional device has been to achieve a thin-film encapsulation.[23] However, the ALD process on organic material, spiro in the present case, is complex due to nonideal surface termination or functionalization and inherent porosity. Here the nucleation process is often substrate-enhanced. This is because the reactant, in particular TMA, infiltrates and is
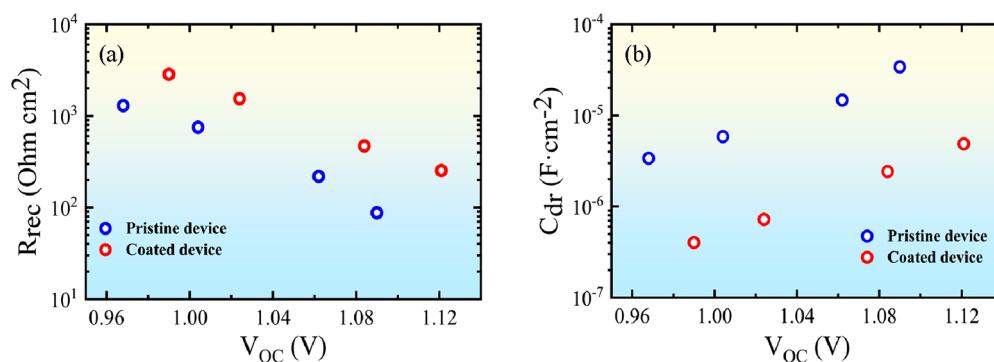
Figure 4. (a) Variation in R_{rec} in pristine (blue) and coated (red) devices. (b) C_{dr} variation in pristine (blue) and coated (red) devices.
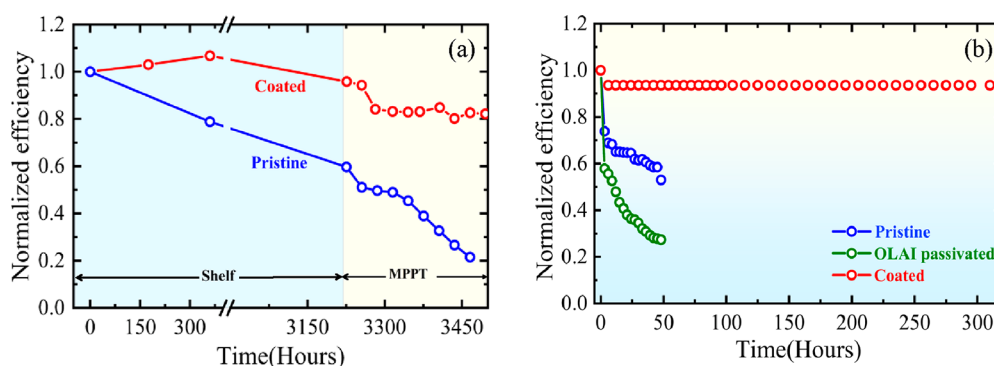

Figure 5. (a) Ambient stability test of pristine and coated devices where blue region shows shelf-stability and yellow region represents continuous operating condition (MPPT) under 100 mW·cm^{-2} illumination. (b) MPPT for pristine (blue), oleylammonium iodide (OLAI) passivated pristine (green), and coated devices (blue) under 10^{-5} Torr vacuum and 100 mW·cm^{-2} illumination.

physisorbed inside the bulk of the organic film,[23] and during the nucleation period, the deposition occurs from the bulk of the organic film. However, due to the relatively lower infiltration of the H_2O molecules in the spiro layer, the Al_2O_3 formation gets limited to the near-surface region, hence leaving TMA molecules to react with the perovskite film at the interface. We have previously shown[15] that the TMA etches the perovskite film by reacting with the organic moiety of the hybrid perovskite and leaves behind PbI_2; the process modifies the stoichiometry at the surface without any effect on the bulk of the material. The detail of the process is schematically explained in Figure S11. Therefore, repeated ALD cycles result in an interfacial PbI_2 layer that is entirely process parameter-dependent (see Figure S12 and the associated discussion). Enhancement of the PbI_2 peak after the ALD coating is determined by the relatively surface-sensitive grazing angle XRD (Figure 3c), while the standard operation under the $\theta-2\theta$ mode does not reveal any change in the PbI_2 peak intensity (Figure 3d). This suggests that the PbI_2 formation is limited only to the interface and only TMA is responsible for its formation (see Figure S13). Considering the architectural similarities, we must mention a recent report on the ALD of amorphous-TiO_2[24] that was deposited on the spiro−metal interface for enhanced hole collection and the ALD of SnO_2[25,26] on a slightly different architecture, but in both of these scenarios, the fundamental aim is to protect ionic diffusion for enhanced stability. However, in the absence of adequate data of the growth mechanism, particularly in the nucleation regime, the generalization of our hypothesis is not prudent. Probabilistically, the metalorganic with a bulkier ligand may or may not diffuse inside the spiro unlike TMA,

discussed here, or the diethyl-zinc (DEZ),[15] but it is too early to draw final conclusions.

To identify the changes in the interfacial electronic properties of the devices, we measured electrochemical impedance spectroscopy (EIS) of the pristine and coated devices, under V_{OC} and with varied illumination intensity. This enables the exploration of different charge concentration conditions as the photogenerated carriers are forced to recombine within the active layer. The Nyquist plots (see Figure S14) reproduced two arcs typical of perovskite solar cells and were fitted with the equivalent circuit (see Figure S15)[27] to extract the relevant parameters. As depicted in Figure S15, the circuit contains three branches in parallel. One branch has the recombination resistance (R_{rec}), considering the transport resistance is negligible in the analyzed samples in comparison to the recombination resistance. Another parallel branch of the circuit contains one capacitor (C_g) which represents the geometrical capacitance corresponding to the device's dielectric behavior, and the third branch includes a resistor (R_{dr}) in series with a capacitor (C_{dr}), which accounts for the ionic effects characteristic of perovskite solar cells and do not contribute at DC conditions. To account for small dispersion deviations, all the capacitors were modeled with constant phase elements keeping the exponents close to unity. While C_g does not present significant differences (see Figure S16a), pointing toward a similar device thickness and overall dielectric properties, the coated sample shows larger R_{rec} values in Figure 4a. Given the good fill-factor for both samples and the better V_{OC} of the coated sample, this R_{rec} difference is attributed to a recombination rate reduction, and thus, the origin can be related to a passivated PbI_2-rich interface in the

Al_2O_3-coated sample that reduces the recombination. It has been previously demonstrated that small amounts of PbI_2 in perovskite devices can passivate the grain boundaries and promote charge transport.[18,19] Combining our observations, we can conclude that the formation of the PbI_2 at the perovskite−HTL interface reduces the interfacial recombination and renders better device V_{OC}. The ALD coating also plays a role in the low-frequency branch under illumination, with a slight increase of R_{dr} (see Figure S16b), particularly evident at higher charge carrier concentration conditions, and a significant decrease of C_{dr} across the whole voltage range (Figure 4b). These observations indicate a reduction of the ionic concentration after the ALD coating, in line with recent drift-diffusion simulations indicating that R_{dr} is not significantly affected by the ionic diffusion coefficient but by the ionic concentration.[28] The reduction of C_{dr}, in contrast, indicates an increase in the ionic mobility. Thus, these results can be interpreted in terms of a reduced ionic intercalation within the surface, as this interface becomes PbI_2-rich in the ALD-coated samples. In contrast, if the mobility of the surface-accumulated ions for the pristine devices is lower but they find a less ionic populated interface, then the buildup of carriers across the interface can also trigger higher interfacial recombination velocity, resulting in higher loss rate constants and reducing the device V_{OC}.

The additive effects of reduced interfacial defects result in an improvement of the overall device stability. Figure 5a shows a comparative performance of the device stability of a representative coated (red) and pristine (blue) device. These devices are subjected to shelf-stability and maximum power point tracking (MPPT), under ambient conditions. For the shelf-stability, the coated device retains 95% of its original efficiency after 3200 h, while for the pristine device, it is ca. 60% (refer to the blue shaded section of Figure 5a). Under the MPPT condition (measured at 60% relative humidity), the coated devices are found to be highly stable after the initial burn-in period and constantly operated for ~300 h at 90% of its starting efficiency while in comparison the pristine device dies down, as clearly depicted in Figure 5a (yellow shaded region). The exclusive advantage of the ALD-coated sample is its operation stability under high vacuum (~10^{-5} Torr), as shown in Figure 5b. It is well reported in the literature that the operational stability of pristine hybrid perovskite devices gets significantly reduced in vacuum due to the degassing of the organic moiety.[29] We find that under continuous operating conditions, the pristine device retains ~60% of its original value after 48 h. The oleylammonium iodide (OLAI) passivated devices are more prone to degradation under similar operating conditions and retain only ~27% of the original value. In contrast, the buried interface passivation by the ALD results in a significantly steady device performance, as shown in Figure 5b. It can be seen that beyond an initial burn-in decay (~6%), the device performance is highly stable in high vacuum, retaining ~94% of its initial value after >300 h, which is otherwise difficult to achieve.

In summary, we have demonstrated that the process of spiro-OMeTAD coating induces a significant level of defects at the interface resulting in nonradiative recombination pathways. We have identified the contribution of these defect states in the overall excited carrier dynamics. Considering the fact that the TMA etches out the organic moiety from the hybrid perovskite and the diffusivity of the reactants through the organic charge transport layer is understandable, we employed the ALD Al_2O_3 coating which passivates the buried interface in a controlled manner by forming PbI_2. The formation of the optimal amount of PbI_2 at the buried HTL−perovskite interface results in the effective removal of the nonradiative recombination centers, and as a consequence, the PL and ELQY are significantly improved; hence, the V_{OC} of the devices is enhanced by ~60−70 mV. Notably, the radiative limit of the V_{OC} of the device is estimated[30] to be 1.34 eV, and the measured V_{OC} under full device illumination is 1.2 eV; hence, the net V_{OC} loss of the device is reduced to 0.12 eV. Our fundamental aim here is to elucidate the underlying root-cause analysis of the effects due to the ALD process. The proposed strategy is simple to execute and provides an effective pathway to improve not only the overall device efficiency but also the operational stability under ambient and, most importantly, under high vacuum conditions as well, which is otherwise challenging. Furthermore, we believe not only that the proposed methodology is important for the perovskite solar cells but also that the resultant understanding can additionally be implemented in other energy devices (such as fuel cells, batteries, etc.) where ALD on polymeric substrates is of concern.

■ ASSOCIATED CONTENT

Ⓢ Supporting Information

The Supporting Information is available free of charge at https://pubs.acs.org/doi/10.1021/acsenergylett.3c00296.

> Experimental details, supplementary device characteristics, PL images, analysis of TRPL, PL spectra analysis, ELQY analysis and discussion, details of the ALD process, and impedance analysis (PDF)

■ AUTHOR INFORMATION

Corresponding Authors

D. D. Sarma − *Solid State and Structural Chemistry Unit, Indian Institute of Science, Bengaluru 560012, India;* ⓞ orcid.org/0000-0001-6433-1069; Email: sarma@iisc.ac.in

Shaibal K. Sarkar − *Department of Energy Science and Engineering, Indian Institute of Technology Bombay, 400 076 Mumbai, India;* ⓞ orcid.org/0000-0001-6788-9738; Email: shaibal.sarkar@iitb.ac.in

Authors

Sudeshna Ghosh − *Center for Research in Nanotechnology and Science, Indian Institute of Technology Bombay, 400 076 Mumbai, India*

Debasmita Pariari − *Solid State and Structural Chemistry Unit, Indian Institute of Science, Bengaluru 560012, India*

Tejmani Behera − *Department of Chemistry, Indian Institute of Technology Bombay, 400 076 Mumbai, India;* ⓞ orcid.org/0000-0003-2995-9293

Pablo P. Boix − *Institut de Ciència dels Materials, University of Valencia, 246980 Paterna, Valencia, Spain;* ⓞ orcid.org/0000-0001-9518-7549

Narasimha Ganesh − *Chemistry and Physics of Material Unit (CPMU), Jawaharlal Nehru Center for Advanced Scientific Research, Bengaluru 560064, India*

Susmita Basak − *Department of Energy Science and Engineering, Indian Institute of Technology Bombay, 400 076 Mumbai, India*

Arya Vidhan − *Department of Energy Science and Engineering, Indian Institute of Technology Bombay, 400 076 Mumbai, India*

Nisha Sarda − *Department of Energy Science and Engineering, Indian Institute of Technology Bombay, 400 076 Mumbai, India*

Iván Mora-Seró − *Institute of Advanced Materials, Universitat Jaume I, 12071 Castelló de la Plana, Spain*

Arindam Chowdhury − *Department of Chemistry, Indian Institute of Technology Bombay, 400 076 Mumbai, India;* ⓘ orcid.org/0000-0001-8178-1061

Kavassery Sureswaran Narayan − *Chemistry and Physics of Material Unit (CPMU), Jawaharlal Nehru Center for Advanced Scientific Research, Bengaluru 560064, India;* ⓘ orcid.org/0000-0001-8550-6868

Complete contact information is available at:
https://pubs.acs.org/10.1021/acsenergylett.3c00296

Notes

The authors declare no competing financial interest.

■ REFERENCES

(1) Green, M. A.; Dunlop, E. D.; Hohl-Ebinger, J.; Yoshita, M.; Kopidakis, N.; Hao, X. Solar cell efficiency tables (version 59). *Progress in Photovoltaics: Research and Applications* **2022**, *30* (1), 3−12.

(2) Lee, D.-K.; Park, N.-G. Materials and Methods for High-Efficiency Perovskite Solar Modules. *Solar RRL* **2022**, *6* (3), 2100455.

(3) Stolterfoht, M.; Caprioglio, P.; Wolff, C. M.; Márquez, J. A.; Nordmann, J.; Zhang, S.; Rothhardt, D.; Hörmann, U.; Amir, Y.; Redinger, A.; et al. The impact of energy alignment and interfacial recombination on the internal and external open-circuit voltage of perovskite solar cells. *Energy Environ. Sci.* **2019**, *12* (9), 2778−2788.

(4) Oliver, R. D. J.; Caprioglio, P.; Peña-Camargo, F.; Buizza, L. R. V.; Zu, F.; Ramadan, A. J.; Motti, S. G.; Mahesh, S.; McCarthy, M. M.; Warby, J. H.; et al. Understanding and suppressing non-radiative losses in methylammonium-free wide-bandgap perovskite solar cells. *Energy Environ. Sci.* **2022**, *15* (2), 714−726.

(5) Zhang, S.; Shaw, P. E.; Zhang, G.; Jin, H.; Tai, M.; Lin, H.; Meredith, P.; Burn, P. L.; Neher, D.; Stolterfoht, M. Defect/Interface Recombination Limited Quasi-Fermi Level Splitting and Open-Circuit Voltage in Mono- and Triple-Cation Perovskite Solar Cells. *ACS Appl. Mater. Interfaces* **2020**, *12* (33), 37647−37656.

(6) Liu, B.; Bi, H.; He, D.; Bai, L.; Wang, W.; Yuan, H.; Song, Q.; Su, P.; Zang, Z.; Zhou, T.; et al. Interfacial Defect Passivation and Stress Release via Multi-Active-Site Ligand Anchoring Enables Efficient and Stable Methylammonium-Free Perovskite Solar Cells. *ACS Energy Letters* **2021**, *6* (7), 2526−2538.

(7) Zhao, R.; Xie, L.; Zhuang, R.; Wu, T.; Zhao, R.; Wang, L.; Sun, L.; Hua, Y. Interfacial Defect Passivation and Charge Carrier Management for Efficient Perovskite Solar Cells via a Highly Crystalline Small Molecule. *ACS Energy Letters* **2021**, *6* (12), 4209−4219.

(8) Gao, F.; Zhao, Y.; Zhang, X.; You, J. Recent Progresses on Defect Passivation toward Efficient Perovskite Solar Cells. *Adv. Energy Mater.* **2020**, *10* (13), 1902650.

(9) Kim, S. Y.; Cho, S. J.; Byeon, S. E.; He, X.; Yoon, H. J. Self-Assembled Monolayers as Interface Engineering Nanomaterials in Perovskite Solar Cells. *Adv. Energy Mater.* **2020**, *10* (44), 2002606.

(10) Ali, F.; Roldán-Carmona, C.; Sohail, M.; Nazeeruddin, M. K. Applications of Self-Assembled Monolayers for Perovskite Solar Cells Interface Engineering to Address Efficiency and Stability. *Adv. Energy Mater.* **2020**, *10* (48), 2002989.

(11) Phung, N.; Verheijen, M.; Todinova, A.; Datta, K.; Verhage, M.; Al-Ashouri, A.; Köbler, H.; Li, X.; Abate, A.; Albrecht, S.; et al. Enhanced Self-Assembled Monolayer Surface Coverage by ALD NiO in p-i-n Perovskite Solar Cells. *ACS Appl. Mater. Interfaces* **2022**, *14* (1), 2166−2176.

(12) Zhang, J.; Yang, J.; Dai, R.; Sheng, W.; Su, Y.; Zhong, Y.; Li, X.; Tan, L.; Chen, Y. Elimination of Interfacial Lattice Mismatch and Detrimental Reaction by Self-Assembled Layer Dual-Passivation for Efficient and Stable Inverted Perovskite Solar Cells. *Adv. Energy Mater.* **2022**, *12* (18), 2103674.

(13) Palmstrom, A. F.; Raiford, J. A.; Prasanna, R.; Bush, K. A.; Sponseller, M.; Cheacharoen, R.; Minichetti, M. C.; Bergsman, D. S.; Leijtens, T.; Wang, H.-P.; et al. Interfacial Effects of Tin Oxide Atomic Layer Deposition in Metal Halide Perovskite Photovoltaics. *Adv. Energy Mater.* **2018**, *8* (23), 1800591.

(14) Das, C.; Kot, M.; Hellmann, T.; Wittich, C.; Mankel, E.; Zimmermann, I.; Schmeisser, D.; Khaja Nazeeruddin, M.; Jaegermann, W. Atomic Layer-Deposited Aluminum Oxide Hinders Iodide Migration and Stabilizes Perovskite Solar Cells. *Cell Reports Physical Science* **2020**, *1* (7), 100112.

(15) Choudhury, D.; Rajaraman, G.; Sarkar, S. K. Self limiting atomic layer deposition of Al_2O_3 on perovskite surfaces: a reality? *Nanoscale* **2016**, *8* (14), 7459−7465.

(16) Koushik, D.; Hazendonk, L.; Zardetto, V.; Vandalon, V.; Verheijen, M. A.; Kessels, W. M. M.; Creatore, M. Chemical Analysis of the Interface between Hybrid Organic−Inorganic Perovskite and Atomic Layer Deposited Al_2O_3. *ACS Appl. Mater. Interfaces* **2019**, *11* (5), 5526−5535.

(17) Petit, R. R.; Li, J.; Van de Voorde, B.; Van Vlierberghe, S.; Smet, P. F.; Detavernier, C. Atomic Layer Deposition on Polymer Thin Films: On the Role of Precursor Infiltration and Reactivity. *ACS Appl. Mater. Interfaces* **2021**, *13* (38), 46151−46163.

(18) Liu, F.; Dong, Q.; Wong, M. K.; Djurišić, A. B.; Ng, A.; Ren, Z.; Shen, Q.; Surya, C.; Chan, W. K.; Wang, J.; et al. Is Excess PbI_2 Beneficial for Perovskite Solar Cell Performance? *Adv. Energy Mater.* **2016**, *6* (7), 1502206.

(19) Chen, Q.; Zhou, H.; Song, T.-B.; Luo, S.; Hong, Z.; Duan, H.-S.; Dou, L.; Liu, Y.; Yang, Y. Controllable Self-Induced Passivation of Hybrid Lead Iodide Perovskites toward High Performance Solar Cells. *Nano Lett.* **2014**, *14* (7), 4158−4163.

(20) Ghosh, S.; Singh, R.; Subbiah, A. S.; Boix, P. P.; Seró, I. M.; Sarkar, S. K. Enhanced operational stability through interfacial modification by active encapsulation of perovskite solar cells. *Appl. Phys. Lett.* **2020**, *116* (11), 113502.

(21) Lin, C.-T.; Lee, J.; Kim, J.; Macdonald, T. J.; Ngiam, J.; Xu, B.; Daboczi, M.; Xu, W.; Pont, S.; Park, B.; et al. Origin of Open-Circuit Voltage Enhancements in Planar Perovskite Solar Cells Induced by Addition of Bulky Organic Cations. *Adv. Funct. Mater.* **2020**, *30* (7), 1906763.

(22) Chen, Y.; Wang, T.; Li, Z.; Li, H.; Ye, T.; Wetzel, C.; Li, H.; Shi, S.-F. Communicating Two States in Perovskite Revealed by Time-Resolved Photoluminescence Spectroscopy. *Sci. Rep.* **2018**, *8* (1), 16482.

(23) Singh, R.; Ghosh, S.; Subbiah, A. S.; Mahuli, N.; Sarkar, S. K. ALD Al_2O_3 on hybrid perovskite solar cells: Unveiling the growth mechanism and long-term stability. *Sol. Energy Mater. Sol. Cells* **2020**, *205*, 110289.

(24) Seo, S.; Shin, S.; Kim, E.; Jeong, S.; Park, N.-G.; Shin, H. Amorphous TiO2 Coatings Stabilize Perovskite Solar Cells. *ACS Energy Letters* **2021**, *6* (9), 3332−3341.

(25) Boyd, C. C.; Cheacharoen, R.; Bush, K. A.; Prasanna, R.; Leijtens, T.; McGehee, M. D. Barrier Design to Prevent Metal-Induced Degradation and Improve Thermal Stability in Perovskite Solar Cells. *ACS Energy Letters* **2018**, *3* (7), 1772−1778.

(26) Zhou, X.; Lai, H.; Huang, T.; Chen, C.; Xu, Z.; Yang, Y.; Wu, S.; Xiao, X.; Chen, L.; Brabec, C. J.; et al. Suppressing Nonradiative Losses in Wide-Band-Gap Perovskites Affords Efficient and Printable All-Perovskite Tandem Solar Cells with a Metal-Free Charge Recombination Layer. *ACS Energy Letters* **2023**, *8* (1), 502−512.

(27) Yoo, S.-M.; Yoon, S. J.; Anta, J. A.; Lee, H. J.; Boix, P. P.; Mora-Seró, I. An Equivalent Circuit for Perovskite Solar Cell Bridging Sensitized to Thin Film Architectures. *Joule* **2019**, *3* (10), 2535−2549.

(28) Riquelme, A. J.; Valadez-Villalobos, K.; Boix, P. P.; Oskam, G.; Mora-Seró, I.; Anta, J. A. Understanding equivalent circuits in perovskite solar cells. Insights from drift-diffusion simulation. *Phys. Chem. Chem. Phys.* **2022**, *24* (26), 15657−15671.

(29) Jiang, Y.; Yang, S.-C.; Jeangros, Q.; Pisoni, S.; Moser, T.; Buecheler, S.; Tiwari, A. N.; Fu, F. Mitigation of Vacuum and Illumination-Induced Degradation in Perovskite Solar Cells by Structure Engineering. *Joule* **2020**, *4* (5), 1087−1103.

(30) Nayak, P. K.; Mahesh, S.; Snaith, H. J.; Cahen, D. Photovoltaic solar cell technologies: analysing the state of the art. *Nature Reviews Materials* **2019**, *4* (4), 269−285.